Supplementary Materials

Selective ROS-mediated oxidative depolymerization of lignin to guaiacyl monomers over a mesoporous Cu_2Fe_1/JN catalyst

Jie Gao[1], Yingxuan Cai[2], Lu Li[2], Jieting Li[2], Yang Cao[3], Yong Guo[4], Pingyi Zhang[2], Xiang Zheng[1], Linxiang Mo[5], Aijun Zhou[5], Jibo Liu[2,*], Haifang Mao[1,*], Shicheng Zhang[6,7*]

[1]Faculty of Flavour Fragrance and Cosmetics, Shanghai Institute of Technology, Shanghai 201418, China.
[2]Faculty of Chemical Engineering and Energy Technology, Shanghai Institute of Technology, Shanghai 201418, China.
[3]College of Engineering, Nanjing Agricultural University, Nanjing 210031, Jiangsu, China.
[4]State Key Laboratory of Green Chemical Engineering and Industrial Catalysis, School of Chemistry and Molecular Engineering, East China University of Science and Technology, Shanghai 200237, China.
[5]Jiaxing Zhonghua Chemical Co., Ltd., Jiaxing 314006, Zhejiang, China.
[6]Shanghai Technical Service Platform for Pollution Control and Resource Utilization of Organic Wastes, Shanghai Key Laboratory of Atmospheric Particle Pollution and Prevention (LAP3), Department of Environmental Science and Engineering, Fudan University, Shanghai 200438, China.
[7]Shanghai Institute of Pollution Control and Ecological Security, Shanghai 200092, China.

[*]**Correspondence to:** Dr. Jibo Liu, Faculty of Chemical Engineering and Energy Technology, Shanghai Institute of Technology, 100 Haiquan Road, Shanghai 201418, China. E-mail: jiboliu@sit.edu.cn; Prof. Haifang Mao, Faculty of Flavour Fragrance and Cosmetics, Shanghai Institute of Technology, Shanghai 201418, China. E-mail: mhf@sit.edu.cn; Prof. Shicheng Zhang, Shanghai Technical Service Platform for Pollution Control and Resource Utilization of Organic Wastes, Shanghai Key Laboratory of Atmospheric Particle Pollution and Prevention (LAP3), Department of

Environmental Science and Engineering, Fudan University, Shanghai 200438, China; Shanghai Institute of Pollution Control and Ecological Security, Shanghai 200092, China. E-mail: zhangsc@fudan.edu.cn

1. Supplementary text

1.1 Chemicals and materials

NaOH (≥98.0%), HCl (36%-38%), NaCl (98.0%), acetic acid (≥99.5%), methanol (≥99.5%), ethanol (≥99.7%), isopropanol (≥99.7%), ethyl acetate (99.5%), sulfuric acid (98.0%), 2-phenoxy-1-phenylethanol (98%), 2-phenoxy-1-phenylethanone (98%), vanillin (99.0%), vanillic acid (98.0%), acetovanillone (98.0%), guaiacol (99.0%), nitrobenzene (98.0%), phenol (99.9), 1-phenylethanol (≥99.0%), acetophenone (≥99.0%), benzoic acid (98%), anhydrous magnesium sulfate (≥98.0%), dichloromethane (99.5%), 5, 5'-dimethyl-1-pyrroline *N*-oxide (≥98.0%), 2,2,6,6-tetramethylpiperidine-1-oxyl (≥ 98.0%), 1,4-benzoquinone (≥ 98.0%), 3,3′,5,5′-Tetramethylbenzidine (98.0%), β-carotene (98.0%), $Cu(NO_3)_2 \cdot 3H_2O$ (99%), and $Fe(NO_3)_3 \cdot 9H_2O$ (98%) were provided by Titan Scientific Co., Ltd (Shanghai, China). JN-30 (30 wt%) were purchased from Jidao Ronghai Jude Fine Chemical Co., Ltd. Calcium lignosulfonate was obtained from Borregaard Co., Ltd. (Shanghai, China). O_2 (≥ 99.999%) and N_2 (≥ 99.999%) were supplied by Shanghai Shenzhong Gas Co., Ltd. All reagents are of analytical grade and were used without further purification. kraft lignin was purchased from Tokyo Chemical Industry Co., Ltd. (Shanghai, China). Organosolv lignins were prepared from wheat using an ethyl acetate/ethanol/water/H_2SO_4 mixture (36.5:24.9:38.1:0.5, w/w). For each extraction, 10.0 g of biomass was suspended in 110 mL of the solvent mixture in a 250 mL sealed high-pressure reactor. After N_2 purging, the suspension was stirred at 300 rpm and heated at 140 °C for 20 min. The reactor was then cooled to room temperature, and the insoluble fraction was removed by filtration. The filtrate was diluted with 100 mL of water and extracted with ethyl acetate (3 × 100 mL). The combined organic extracts were dried over anhydrous $MgSO_4$, filtered, and concentrated under reduced pressure to afford the organosolv lignin.

1.2 Catalyst characterizations

Scanning electron microscopy (SEM) and transmission electron microscopy (TEM)

was employed to characterize catalyst morphology. SEM was recorded on a ZEISS Sigma 300 microscope. Transmission electron microscopy (TEM) images were recorded on a Hitachi HT7700 Exalens microscope. High-resolution TEM (HRTEM) images were obtained on a FEI Tecnai G2 F20 S-Twin microscope. Energy dispersive X-ray spectroscopy (EDS) analyses were performed on Oxford X-Max 80T energy dispersive X-ray spectrometer detector. N_2 adsorption isotherms were collected to evaluate the specific surface area and porous structure of the catalysts at -196 °C on a Micromeritics ASAP 2460 analyzer. Brunauer-Emmett-Teller (BET) model was adopted to calculate the specific surface area (S_{BET}). The total pore volume (V_t) was determined from the amount of N_2 adsorbed at a relative pressure (P/P_0) of ~0.99, while pore size distributions were determined via density functional theory (DFT) fitting of adsorption data. Inductively coupled plasma optical emission spectroscopy (ICP-OES) was carried out to measure Cu and Fe content by using vario EL III instruments. Powder X-ray diffraction (XRD) patterns were measured on a Rigaku Ultimate IV diffractometer with Cu Ka radiation (40 kV, 40 mA, λ = 1.5418 Å). The patterns were recorded over a scanning angle (2θ) range of 10º to 80º at a scan speed of 5 º/min. X-ray photoelectron spectroscopy (XPS) was performed on a Thermo Fisher Scientific ESCALAB 250Xi instrument to determine the surface chemical states of Cu, Fe, and O. All spectra were charge-corrected by referencing the adventitious C 1s peak to 284.8 eV. High-resolution spectra were fitted using a Shirley-type background and mixed Gaussian-Lorentzian (GL) line shapes. The peak positions and full widths at half maximum (FWHMs) were constrained within physically reasonable ranges. Specifically, the FWHM values of all fitted characteristic peaks were limited in the range of 1.0-2.5 eV, and the binding energy positions of Cu 2p, Fe 2p, and O 1s peaks were restricted within the standard elemental and chemical state reference ranges of ± 0.2 eV. Consistent fitting constraints were applied to ensure reliable and reproducible peak assignments. H_2 temperature-programmed reduction (H_2-TPR) experiments were carried out on a Micromeritics AutoChem II 2920 apparatus. Typically, 60 mg catalyst was loaded in a quartz reactor and pretreated at 200 °C under flowing Ar (30 mL/min) for 1 h to eliminate surface contaminants and adsorbed water. After cooling down to 80 °C, the reactor was purged with a H_2/Ar mixture (30 mL/min). Subsequently, the sample was ramped to 700 °C at 10 °C/min under Ar atmosphere, and the thermal conductivity

detector (TCD) continuously recorded gaseous signals. NH_3-temperature-programmed desorption (NH_3-TPD) experiments were carried out on a Micromeritics AutoChem II 2920 apparatus. Typically, 60 mg catalyst was loaded in a quartz reactor and pretreated at 200 °C under flowing He (30 mL/min) for 1 h to eliminate surface contaminants and adsorbed water. After cooling down to 50 °C, the reactor was purged with a NH_3/He mixture (30 mL/min). Subsequently, the sample was ramped to 700 °C at 10 °C/min under He atmosphere, and the thermal conductivity detector (TCD) continuously recorded gaseous signals.

1.3 Substrate accessibility experiment

The effect of the mesoporous structure of Cu_2Fe_1/JN on substrate accessibility was evaluated using 2-phenoxy-1-phenylethanol as a representative β-O-4 model compound. In a typical experiment, 2-phenoxy-1-phenylethanol (0.210 g), Cu_2Fe_1/JN (0.025 g), and NaOH solution (50 mL, 1.25 M) were placed in a flask and stirred at 100 °C under a N_2 atmosphere at 500 rpm. Aliquots were collected at predetermined intervals. The catalyst was rapidly removed, and the concentration of 2-phenoxy-1-phenylethanol was quantified by HPLC. A catalyst-free control was performed under otherwise identical conditions to account for substrate loss caused by thermal or alkaline treatment.

1.4 Catalyst recyclability experiment

The recyclability of Cu_2Fe_1/JN was evaluated in the catalytic oxidation of 2-phenoxy-1-phenylethanol under the standard reaction conditions. After completion of each reaction cycle, the catalyst was separated from the reaction mixture by centrifugation, thoroughly washed with deionized water to remove residual alkaline species and soluble reaction products, and subsequently dried before reuse. The recovered catalyst was directly used for the next catalytic cycle. This procedure was repeated for consecutive cycles to evaluate the catalytic stability and recyclability of Cu_2Fe_1/JN. The product yield was determined by HPLC after each cycle.

1.5 Products analysis

After the reaction, the catalyst was isolated by filtration. The filtrate was acidified to pH 2 with dilute HCl (2 mM) and subsequently extracted three times with ethyl

acetate (25 mL each). The combined organic extracts were dried over anhydrous Na_2SO_4 before instrumental analysis. The liquid products were identified using a gas chromatograph-mass spectrometer (GC-MS, Agilent TRACE 1600) equipped with a TG-624SiMS capillary column (30 m × 0.25 mm i.d. × 0.14 μm). Helium was employed as the carrier gas at a constant flow rate of 1.0 mL/min. The oven program started at 50 °C and was held for 5 min, followed by heating to 240 °C at 10 10 °C/min and a final hold of 11 min. Samples (1 μL) were injected for analysis, and chromatographic data were processed using Thermo Scientific workstation software. Quantitative analysis was further performed on an high-performance liquid chromatography (HPLC) system (Thermo Fisher Scientific Vanquish) fitted with a C18 column (5 μm, 120 Å, 4.6 × 250 mm) and a UV detector operating at 280 nm. The mobile phase consisted of HPLC-grade methanol and 0.1% phosphoric acid aqueous solution (solvent B), using a methanol/water composition of 20:80 (v/v). The separation was carried out at 25 °C with a flow rate of 1.0 mL/min. The yield of each identified product was calculated according to Eq. (1). The relative G-derived aromatic monomers yield (RGY) was calculated as the ratio of the experimental G-derived aromatic monomers yield to the theoretical G-derived aromatic phenolic monomers yield estimated from NBO analysis (Eq. 2).

$$\text{Yield}\ (\%) = W_{\text{single product}}/W_{\text{lignin}} \times 100\% \quad (1)$$

$$\text{RGY}(\%) = W_{\text{G-derived aromatic monomers from this system}}/W_{\text{G-derived aromatic monomers from NBO}} \times 100 \quad (2)$$

1.6 Investigation of ROS generation, speciation, and contributions

In-situ UV-vis light fluorescence spectra were collected using a UV-Vis DRS (UH4150, Thermo Fisher Scientific, USA) equipped with a 9.5 mm × 1.5 mm silver halide fiber probe and a diamond probe tip. Moreover, electron paramagnetic resonance (EPR) measurements were performed on a Bruker EMXnano spectrometer.

1.7 Lignin Characterization and Evolution during Reaction

Fourier Transform Infrared Spectrometry (FTIR, NICOLET iS10 SMART iTR) was applied to investigate the structure of the lignin. Each sample was scanned 32 times from 4000 to 500 cm^{-1} with a resolution of 0.4 cm^{-1}. The structural evolution of lignin

during depolymerization was monitored by in-situ FTIR spectroscopy using a Mettler Toledo ReactIR 15 system equipped with a liquid nitrogen-cooled MCT detector. The FTIR spectra were continuously collected at 30 s intervals over the range of 1800-1000 cm^{-1}. In-situ UV-vis spectroscopy was further employed to track the changes in lignin during the reaction. The measurements were conducted on a UH4150 UV-vis spectrophotometer (Thermo Fisher Scientific) equipped with a Process Eye-Multi Spec probe, and spectra were recorded at predefined time intervals within the wavelength range of 185-450 nm.

2. Supplementary Figures and Tables

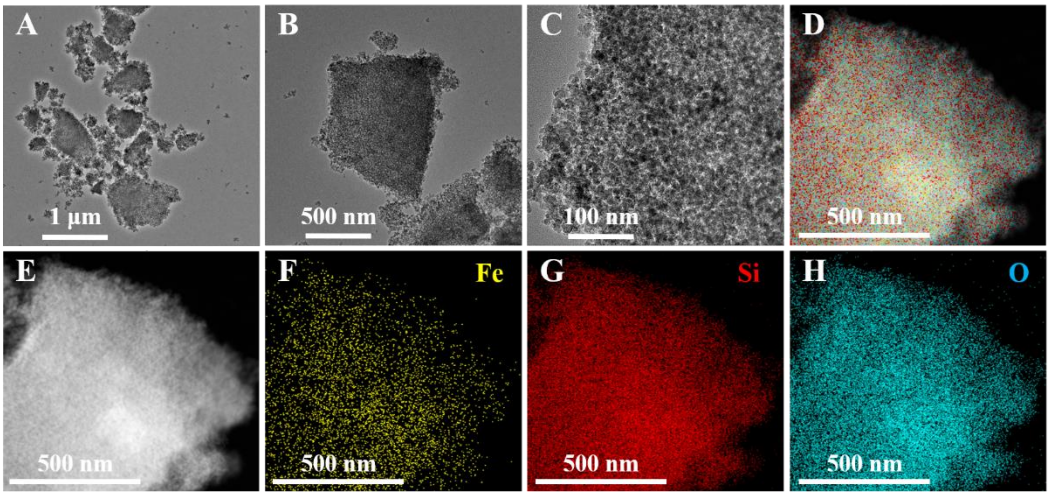

Supplementary Figure 1. (A-C) TEM images. (D-H) Corresponding energy-dispersive X-ray (EDX) elemental mapping of overlapped image and Fe, Si, O element of Fe/JN.

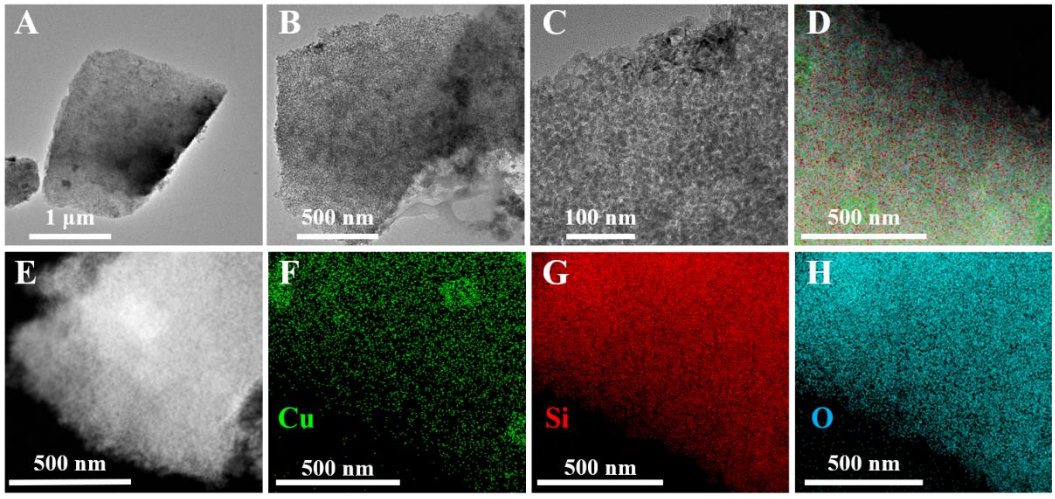

Supplementary Figure 2. (A-C) TEM images. (D-H) Corresponding energy-dispersive X-ray (EDX) elemental mapping of overlapped image and Cu, Si, O element of Cu/JN.

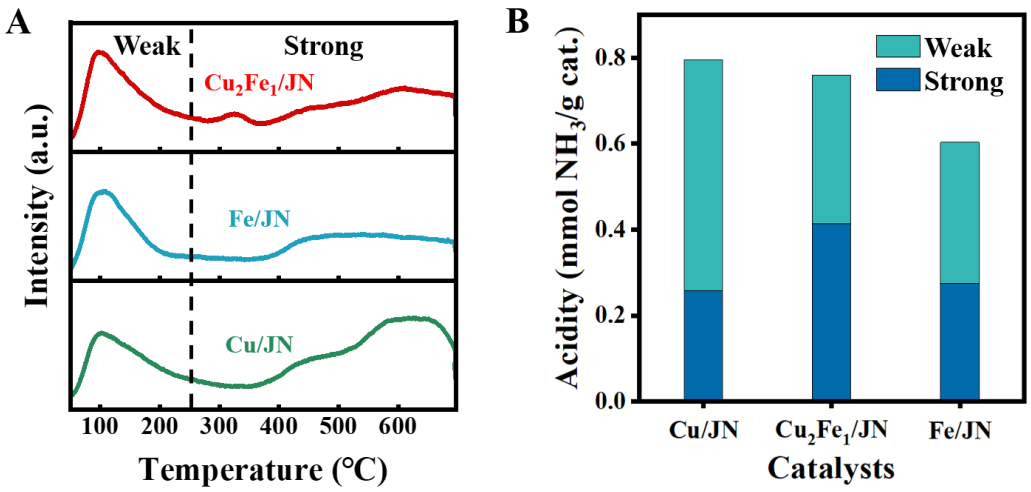

Supplementary Figure 3. (A) NH_3-TPD profiles of Cu_2Fe_1/JN, Cu/JN, and Fe/JN. (B) the acidity distribution of Cu_2Fe_1/JN, Cu/JN, and Fe/JN.

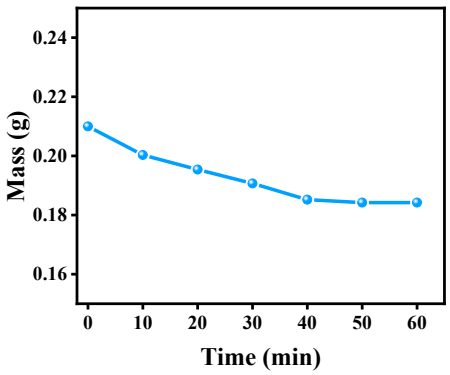

Supplementary Figure 4. Time-dependent adsorption of 2-phenoxy-1-phenylethanol over Cu_2Fe_1/JN.

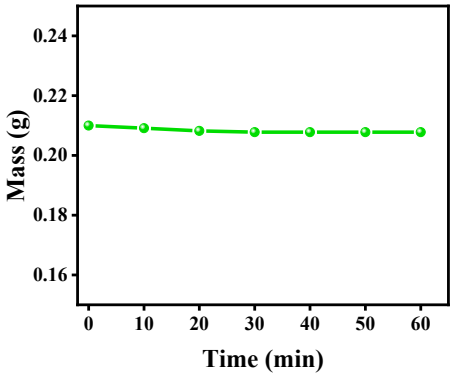

Supplementary Figure 5. Time-dependent adsorption of 2-phenoxy-1-phenylethanol in the catalyst-free control.

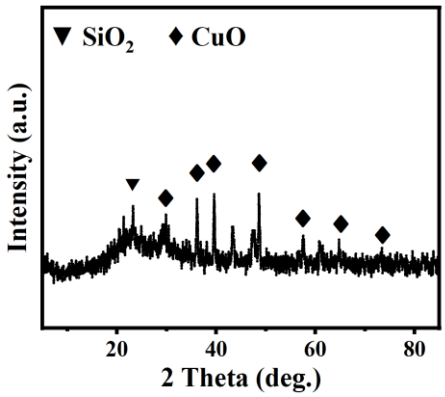

Supplementary Figure 6. XRD pattern of the spent Cu_2Fe_1/JN.

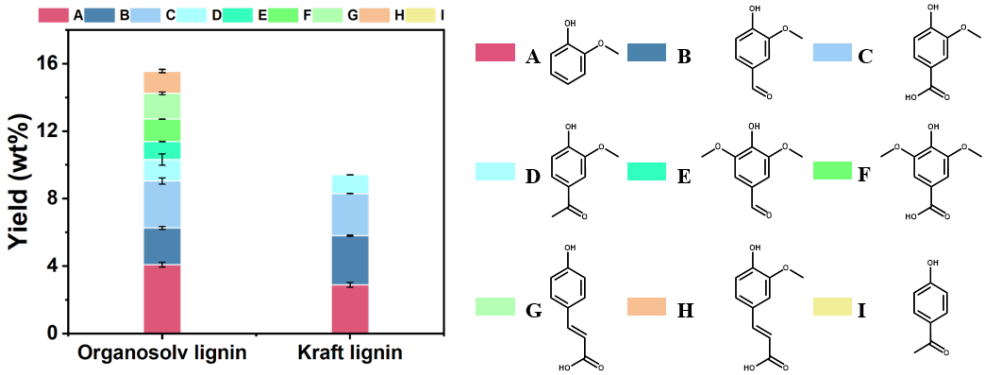

Supplementary Figure 7. Cu_2Fe_1/JN catalyzed monomer yield for different lignin. Reaction conditions: 2.5 g lignin, 0.25 g Cu_2Fe_1/JN, 1.25 M NaOH, 0.4 MPa O_2, 50 mL water, 150 °C, 5 h. The data was the mean ± standard deviation (N = 3).

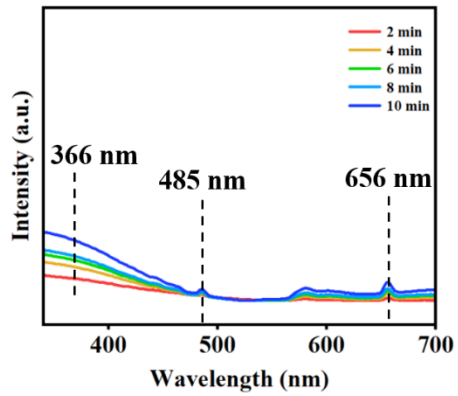

Supplementary Figure 8. Time-dependent UV-vis spectra of TMB oxidation over Cu/JN.

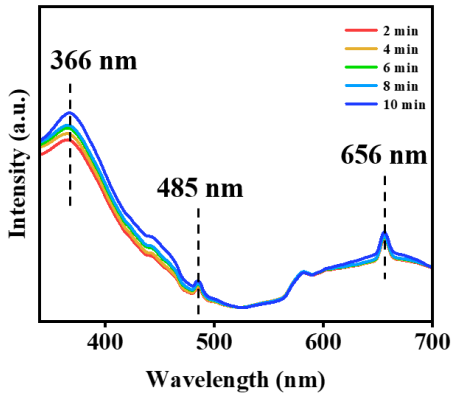

Supplementary Figure 9. Time-dependent UV-vis spectra of TMB oxidation over Fe/JN.

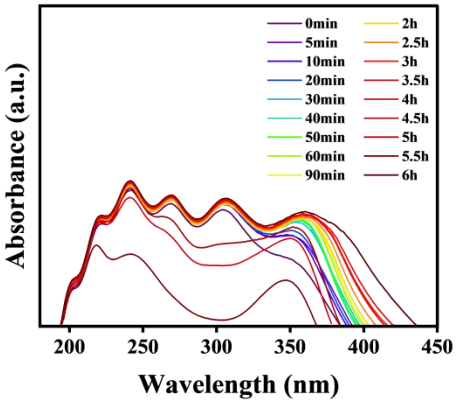

Supplementary Figure 10. Time-dependent UV-vis spectra and corresponding 2D contour plots of calcium lignosulfonate during oxidative depolymerization over Cu/JN.

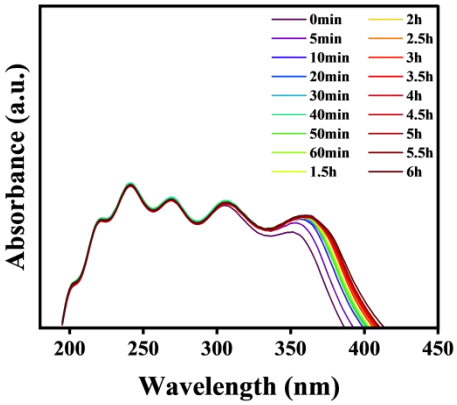

Supplementary Figure 11. Time-dependent UV-vis spectra and corresponding 2D contour plots of calcium lignosulfonate during oxidative depolymerization over Fe/JN.

Supplementary Table 1. **Cu and Fe loadings of various catalysts determined by ICP-OES**

Entry	Catalyst	Cu loading (wt%)	Fe loading (wt%)
1	Cu_2Fe_1/JN	12.7	6.7
2	Cu/JN	19.4	0.0
3	Fe/JN	0.0	20.8
4 [a]	Cu_2Fe_1/JN	11.9	6.5

[a] Cu_2Fe_1/JN catalyst after three cycles under the optimized conditions.

Supplementary Table 2. Relative concentrations of Cu^{2+} and Cu^{+} derived from the Cu 2p XPS spectra of the catalysts

Entry	Catalyst	Relative atomic percentage (%)					
		Cu^{2+} $2p_{3/2}$	Cu^{+} $2p_{3/2}$	Cu^{2+} $2p_{1/2}$	Cu^{+} $2p_{1/2}$	Cu^{2+}	Cu^{+}
1	Cu_2Fe_1/JN	27.8	41.2	9.5	21.5	37.3	62.7
2	Cu/JN	27.3	40.5	12.3	19.8	39.7	60.3

Supplementary Table 3. Relative concentrations of Fe^{3+} and Fe^{2+} derived from the Fe 2p XPS spectra of the catalysts

Entry	Catalyst	Relative atomic percentage (%)					
		Fe^{3+} $2p_{3/2}$	$Fe^{2+}2p_{3/2}$	$Fe^{3+}2p_{1/2}$	$Fe^{2+}2p_{1/2}$	Fe^{3+}	Fe^{2+}
1	Cu_2Fe_1/JN	31.0	29.6	16.4	23.0	47.4	52.6
2	Fe/JN	28.5	30.7	16.9	23.9	45.4	54.6

Supplementary Table 4. Relative concentrations of O_{ads}, O_{vac}, and O_{latt} derived from the O 1s XPS spectra of the catalysts

Entry	Catalyst	Relative atomic percentage (%)		
		O_{ads}	O_{vac}	O_{latt}
1	Cu/JN	19.1	72.8	8.2
2	Cu_2Fe_1/JN	19.9	68.6	11.4
3	Fe/JN	13.7	68.7	17.6

Supplementary Table 5. **Yields of products obtained from the nitrobenzene catalyzed oxidation of calcium lignosulfonate**

Entry	Oxidant	Yield of products (%)				
						
1[a]	nitrobenzene	2.1	0.7	10.59	0.2	0.9

[a] NBO oxidation method: 0.15 g calcium lignosulfonate, 2 mL nitrobenzene, 38 mL 2 mol/L NaOH, 170 °C, N_2, 3 h.

Supplementary Table 6. Comparison of catalytic results over different catalysts in the depolymerization of lignin

Entry	Catalyst	G-type products yield (%)	Oxidant	Temp. (°C)	Time (h)	Ref.
1	CuO/TiO_2	8.0	Air	150	0.5	[1]
2	[BSHMIM]-$H_2PMo_{12}O_{40}$	6.5 (64.5mg/g)	O_2	180	1	[2]
3	$LaFe_{0.2}Cu_{0.8}O_3$	6.4	O_2	160	2	[3]
4	$Sr(OH)_2$	5.8	Air	175	0.17	[4]
5	KH_4PMoV_2	2.8	O_2	140	10	[5]
6	Cu_2Fe_1/JN	10.4	O_2	150	5	This work

Supplementary Table 7. Yields of products obtained from the oxidation of calcium lignosulfonate

Entry	Oxidant	Base	Yield of products (%)		
					
1[a]	O_2	/	0.2	0.3	0.4
2[b]	/	NaOH	0.2	0.1	n.d.

[a]Reaction conditions: 2.5 g calcium lignosulfonate, 0.25 g Cu_2Fe_1/JN, 0 M NaOH, 0.4 MPa O_2, 50 mL water, 150 °C, 5 h.

[b] Reaction conditions: 2.5 g calcium lignosulfonate, 0.25 g Cu_2Fe_1/JN, 1.25 M NaOH, 0.4 MPa N_2, 50 mL water, 150 °C, 5 h.

REFERENCES

(1) Vilcocq, L.; Chaussard, N.; Hernández Mañas, A.; Boyron, O.; Taam, M.; Bertaud, F.; Fongarland, P.; Djakovitch, L., Potential of catalytic oxidation of kraft black liquor for the production of biosourced compounds. *Green Chem.* **2023,** *25*, 4793-4807. DOI: 10.1039/d3gc00388d

(2) Wang, D.; Cui, M.; Zhao, W.; Zhang, J.; Liu, M.; Chen, S.; Liu, X.; Li, Y.; Ma, S.; Wei, X.-Y., Selective Oxidation Cleavage of Cα-Cβ Bonds between Lignin Aromatic Units via Phosphomolybdic Acid-Ionic Liquid. *J. Agric. Food. Chem* **2025,** *73*, 12821-12833. DOI: 10.1021/acs.jafc.4c12211

(3) Li, Y.; Zhu, J.; Zhang, Z.; Qu, Y., Preparation of Syringaldehyde from Lignin by Catalytic Oxidation of Perovskite-Type Oxides. *ACS Omega* **2020,** *130*, 2107-2113. DOI: 10.1021/acsomega.9b02379

(4) Kruger, J. S.; Dreiling, R. J.; Wilcox, D. G.; Ringsby, A. J.; Noon, K. L.; Amador, C. K.; Brandner, D. G.; Ramirez, K. J.; Haugen, S. J.; Klein, B. C.; Davis, R.; Hanes, R. J.; Happs, R. M.; Cleveland, N. S.; Christensen, E. D.; Miscall, J.; Beckham, G. T., Lignin alkaline oxidation using reversibly-soluble bases. *Green Chem.* **2022,** *24*, 8733-8741. DOI: 10.1039/d2gc03333j

(5) Wang, X.; Liu, S.; Gao, Y.; Li, G.; Li, Y.; Xu, W.; Qu, Z.; Zhang, L.; Wu, J.; Huo, M., Metal-Substituted Vanadium-Based Polyoxometalate Catalysts for Catalytic Oxidation of Lignin: Activity and Reaction Mechanism. *J. Phys. Chem. C* **2026,** *130*, 3336-3347. DOI: 10.1021/acs.jpcc.5c08738